Residual Stress Simulation for Hot Strip Bimetallic Roll during Quenching

Nao-Aki Noda,* Kejun Hu, Yoshikazu Sano, Katsma Ono, and Yusuke Hosokawa

Bimetallic rolls are widely used in hot rolling mills because of excellent hardness, wear resistance, and high temperature properties. Considerable residual stresses are produced for the bimetallic roll during quenching. Moreover, severe thermal stresses are caused by heating-cooling thermal cycles during subsequent hot rolling process. Fracture from the roll center may occur due to the residual stress adding to the thermal stress, and therefore, it is desirable to investigate the residual stress to improve roll service life. Therefore, FEM simulation of the bimetallic roll is performed for the quenching process. It should be noted that a large number of experimental data of the core and shell material are utilized for the wide range of temperature considering the quenching. The generation mechanism for the residual stress is discussed focusing on the effect of temperature gradient and phase transformation. Furthermore, the effects of shell–core ratio and diameter on residual stress are considered. Results show that the residual stress only slightly increases with increasing shell–core ratio, while significantly increases with increasing diameter.

1. Introduction

Work rolls are used in the roughing stands of hot strip mill to reduce the steel thickness. They have to meet the requirements of hardness, wear resistance at the surface, and toughness at the center.[1–3] Traditional single material roll cannot satisfy these conflicting properties at the same time. Many studies have been done to improve roll performance in the past decades. The bimetallic roll is one of the most important developments to resolve above problem.[4,5] Among them, high speed steel (HSS) is widely used in the bimetallic roll as shell material. The HSS roll is characterized by excellent hardness, good wear resistance of shell material, and significant toughness of core material.[6–9] As shown in **Figure 1**, the bimetallic roll is manufactured by centrifugal casting method, using HSS as shell material and the ductile casting iron (DIC) as core material.

During heat treatment, residual stress is inevitably introduced due to temperature gradient and phase transformation.[4,10,11] The residual stress is self-equilibrating within the roll, independent of the any external loads. In addition, thermal stress is produced by heating-cooling thermal cycles during subsequent hot rolling process.[12–15] The existing residual stress will be added to thermal stress, leading to roll fracture. In order to prevent the thermal crack caused by thermal behavior, suitable compressive stresses are necessary at the roll surface.[16] However, the tensile stress appearing at the center may cause the risk of fracture from the inside of the roll, whose distribution has not been investigated until now.

The stable quality of the work roll is closely related to the quality of rolling product and manufacture cost.[9,12] Therefore, the investigation of the residual stress is necessary and urgent in order to improve service life of the work roll.

2. Previous Studies for Residual Stress of Work Rolls

In most previous studies, the residual stress was measured experimentally. Many practical measuring methods were proposed for residual stress.[17] Destructive mechanical methods include deep hole drilling method, Sachs boring method and slitting method,[18–21] and non-destructive methods include X-ray diffraction method and Ultrasonic method.[22,23] However, the experimental methods are time-consuming, high cost, and even have to damage experimental components. Especially for large-scale bimetallic roll, destructive methods are always limited by measuring accuracy and non-destructive methods are limited by measuring depth.

[*] N.-A. Noda, K. Hu, Y. Sano, K. Ono, Y. Hosokawa
1-1 Department of Mechanical Engineering, Kyushu Institute of Technology, Sensui-cho, Tobata-ku, Kitakyushu-shi, Fukuoka, 804-8550, Japan
Email: noda@mech.kyutech.ac.jp

DOI: 10.1002/srin.201500430

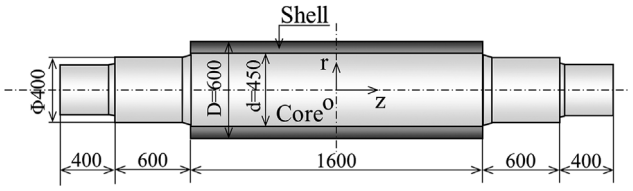

Figure 1. Schematic diagram of the HSS bimetallic roll (mm).

Despite a number of studies focused on residual stress caused by quenching in the past decades, most studies dealt with small size components.[24–27] Recently, Torres et al.[28] analyzed bimetallic work rolls during post casting cooling stage. Although they have studied the prediction of the residual stress on the high chrome steel roll, the most critical quenching process has not been covered yet.

To analyze quenching process, a large amount of material properties are necessary regarding two different materials in the bimetallic roll. Those data have to be obtained under the wide range of temperature including high-temperature region which are difficult to be obtained. In this study, the experimental data are obtained along the same temperature process of quenching to ensure the accuracy of simulation.

In this study, a thermo-elastic-plastic finite element simulation will be performed by using MSC.Marc2012 to investigate the residual stress during quenching. In the first place, the simulation of bimetallic roll will be performed to investigate the generation mechanism and distribution of residual stress. Then, the effects of the shell–core ratio, diameter, phase transformation, and material heat treatment process on the residual stress will be discussed.

3. Quenching Process and FEM Analysis of Bimetallic Rolls

3.1. HSS Bimetallic Rolls

The HSS bimetallic rolls with diameter of 600 mm, body length of 1600 mm and shell thickness of 75 mm, consist of the high speed steel as outer layer and the ductile iron as inner layer and roll neck as shown in Figure 1. **Table 1** shows the chemical compositions of high speed steel and ductile casting iron for the common HSS bimetallic rolls, and **Table 2** shows the material properties of high speed steel and ductile casting iron at room temperature.

3.2. Experimental Section

3.2.1. Tensile Test

The tensile test was conducted by using a standard testing machine INSTRON 5587 with the tensile speed 2.5% min^{-1}. The specimens shown in **Figure 2** were prepared from HSS bimetallic roll. The specimens were heated up to T_{Start} with the speed of 500 °C h^{-1}, then, cooled down to the testing temperature including room temperature, and $T_{Start} - 100$ °C at the interval of 100 °C. The cooling speeds of the specimens were the same as the speeds of roll quenching. The specimens were kept at the testing temperature for 20 min after cooling process.

3.2.2. Dilatometric Experiment

The tests are conducted by using thermal mechanical analysis method.[29] The specimens were prepared from HSS bimetallic roll, with 8 mm thickness, 8 mm width, and 17 mm length. The cooling speed is the same as the one of quenching without considering keeping temperature process of real roll in **Figure 3**(a). The test temperature was in the region from T_{Start} to room temperature.

3.3. Heat Treatment

Figure 3(a) shows the schematic diagram of the heat treatment process including pre-heating, quenching and tempering. In pre-heating process, the whole roll is heated up to the uniform temperature of T_{Start} and kept for several hours. Then, the roll temperature drops rapidly through air cooling. After that the roll is put into the furnace again and maintained at T_{Keep1} to prevent excessive thermal stresses caused by rapid cooling. After keeping period, the roll is cooled down slowly until to the temperature of T_{Finish}.

Composition	C	Si	Mn	P	S	Ni
HSS	1–3	<2	<1.5			<5
DCI	2.5–4	1.5–3.1		<0.1	<0.1	0.4–5

Cr	Mo	Co	V	W	Mg
2–7	<10	<10	3–10	<20	<10
0.01–1.5	0.1–1				0.02–0.08

Table 1. Chemical compositions of high speed steel and ductile iron for high speed steel roll /mass%.

Property	HSS	DCI
0.2% proof stress [MPa]	(1282)[a)]	415
Young's modulus [GPa]	233	173
Poisson's ratio	0.3	0.3
Density [kg m^{-3}]	7.6	7.3
Thermal expansion coefficient [K^{-1}]	12.6×10^{-6}	13.0×10^{-6}
Thermal conductivity [W (m k)$^{-1}$]	20.2	23.4
Specific heat [J (kg K)$^{-1}$	0.46	0.46

[a)]Tensile strength of the shell material is indicated as the 0.2% proof stress became the deformation at break is small.

Table 2. Mechanical properties of high speed steel and ductile casting iron at room temperature.

After quenching process, the tempering process will be performed 2–4 times to release the residual stress and obtained the stable microstructure. The effect of tempering process is not considered in this study and will be studied in the future.

3.4. FEM Analysis

In this study, the MSC.Marc 2012 software is used to carry out FEM elastic-plastic analysis to simulate the quenching process for HSS bimetallic rolls. Figure 3(b) shows the axisymmetric FEM model of HSS bimetallic roll. The roll clutch with the length of 400 mm is ignored because of the small effect on the residual stress at the central section. A 4-node linear axisymmetric quad element with the mesh size of 5×5 mm is adopted for the transient-static simulation. The displacement boundary conditions and thermal isolation conditions are applied to $z = 0$ due to the symmetry. In this study, roll surface temperature $T_{surface}$ obtained by measuring experimentally is imposed to the roll surface.

At the beginning of this study, the heat transfer coefficient was obtained to confirm the FEM result. In this case, since the heat transfer coefficient depends on many factors, such as, material, size, surface conditions of a part, the accurate heat transfer coefficient can be obtained in the following way. First, a value of heat transfer coefficient is assumed from the reference and applied to the roll surface. Second, $T_{Ambient}$ is applied to FEM model of the roll, then roll surface temperature $T_{Simulation}$ is obtained by the simulation and compared with $T_{surface}$. Here, the ambient temperature $T_{Ambient}$ is obtained by measuring experimentally. Third, the reference heat transfer coefficient is changed repeatedly if $T_{Simulation} \neq T_{Surface}$. The real heat transfer coefficient is finally obtained when $T_{simulation} = T_{Surface}$. The calculated heat transfer coefficients including effect of radiation are shown in Figure 3(c).

A large amount of material properties of the shell and core materials have to be measured from T_{Start} to T_{Finish} at a certain interval of temperature. Then, they are used in the simulation as input data. Those material properties include Young's modulus, thermal expansion, specific heat, density, yield point, thermal conductivity, and Poison's ratio. In this paper, those material data in Figure 3, 4, 9, 10, and 11, cannot be indicated in detail because they are confidential data of the roll manufacturing company. According to the custom of this industrial field, the chemical composition, dissolution method, casting conditions, and heat treatment, especially the high temperature properties, are regarded as the trade secret belonged to the owner. In this paper, therefore, the dimensionless values have to be used to characterize the material properties heat treatment process. Since, the purpose of this paper is to clarify the residual stress during quenching process, the simulation results are still useful enough for the readers to understand the generation mechanism and the residual stress distribution.

3.5. Residual Stress Generation Mechanism for HSS Bimetallic Rolls

Figure 4 shows the histories of (a) temperature, (b) stress σ_z, and (c) Young's modulus for the bimetallic roll during quenching process. Since, FEM elastic-plastic analysis needs Young's modulus even under high temperature, a specific stress point is focused when the strain reaches

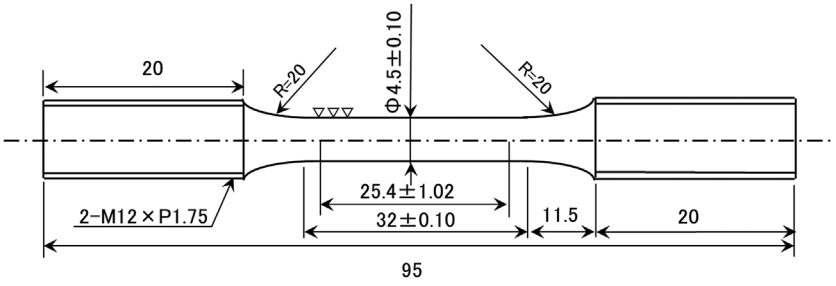

Figure 2. Specimen of the tensile test (mm).

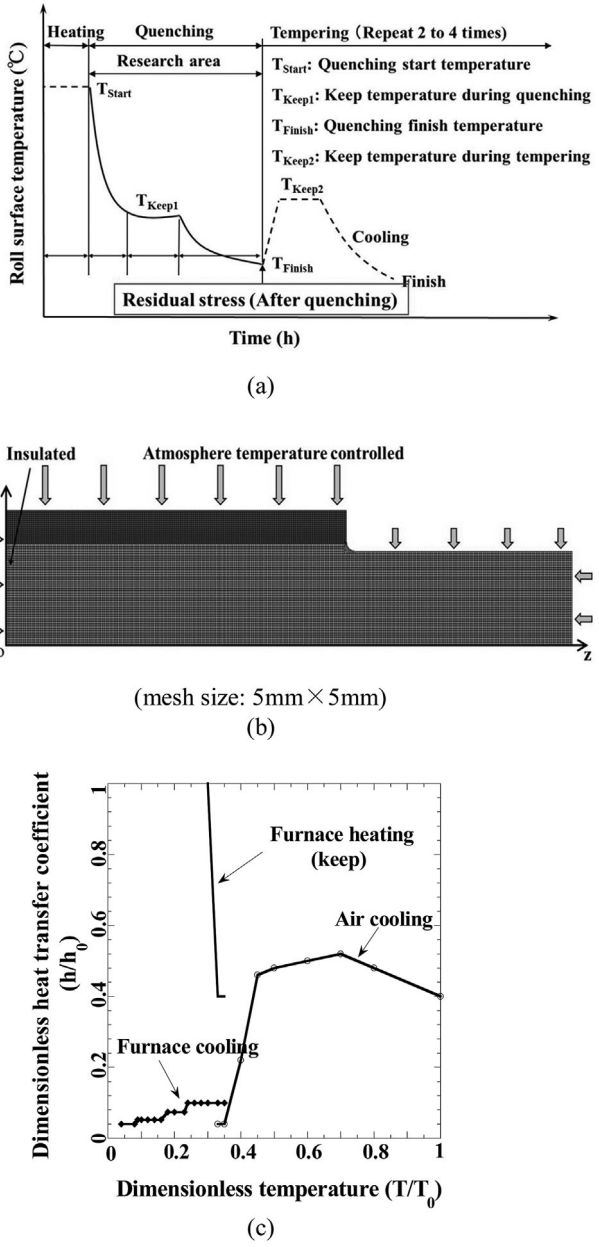

Figure 3. The FEM analysis of HSS bimetallic rolls during quenching: a) heat treatment process; b) FEM model and boundary; and c) heat transfer coefficients.

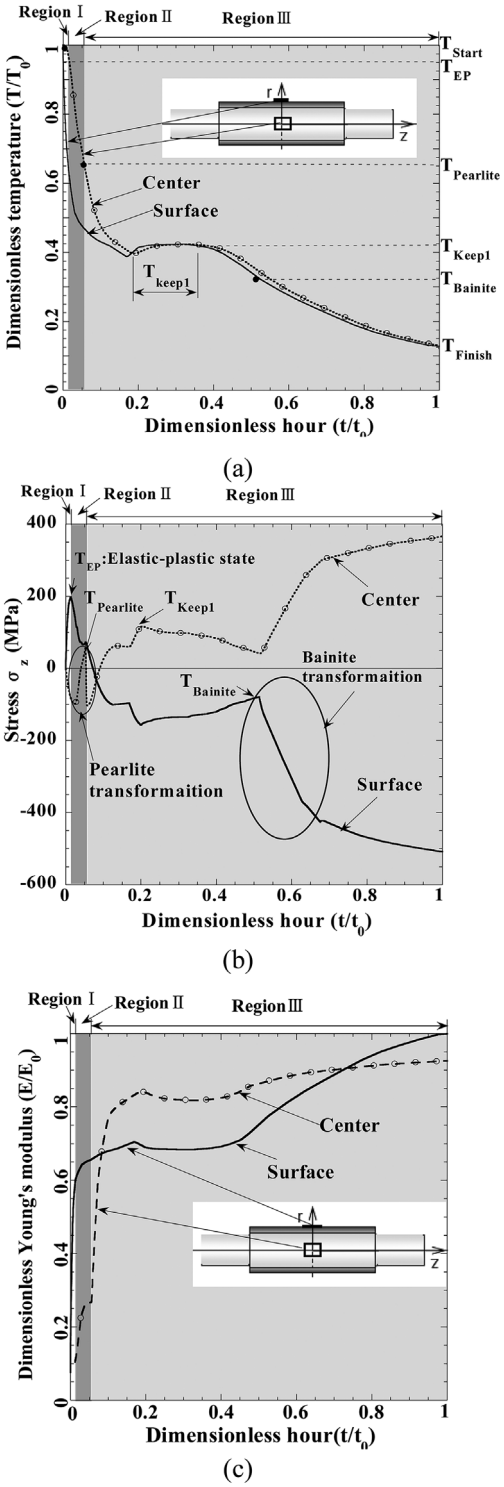

Figure 4. Residual stress generation mechanism of the bimetallic roll: a) temperature histories; b) stress σ_z histories; and c) Young's modulus histories.

0.05% on the stress–strain curve. Then, the Young's modulus is defined as the gradient of the line connecting the origin and the specific point. Figure 4(c) shows the Young's modulus during quenching process, which varies depending on temperature.

The quenching process is divided into RegionI, Region II, and Region III classified by the dominant elastic or plastic state at the surface and center. In the Region I, the yield strength of shell and core is very low due to high temperature, the stress rapidly increases and exceeds the yield stress. Therefore, the large plastic deformation occurs at both roll surface and roll center. In the Region II, since the surface becomes elastic due to surface cooling, the surface Young's modulus increases with decreasing temperature although the center still keeps high

temperature and plastic state. In the Region III, since both surface and the center become elastic, both Young's modulus increases as the cooling continues.

The initial residual stress before quenching can be eliminated because of the pre-heating to high temperature of T_{Start}. In the Region I, the roll is cooled down from T_{Start}, the surface temperature rapidly drops. As a result, tensile stress is produced at the surface and compressive stress is produced at the center.

In the Region II, at the temperature of T_{EP}, the surface changes into elastic-plastic while the center still keeps plastic. In addition, the dropping speed of surface temperature decreases. As a result, the center thermal contraction becomes larger than surface thermal contraction, leading to the stresses at the center and the surface decrease. As center temperature dropping to the temperature of $T_{Pearlite}$, pearlite transformation happens near the boundary and expands toward the center. In this period, the center is shrunk relative to the other parts of the core which expand gradually due to pearlite transformation. Hence, the compressive stress at the center decreases until becomes tensile stress. The tensile stress reverses to compressive stress rapidly when the pearlite transformation reaches to the center.

In the Region III, the center is further contracted relative to the surface because of larger temperature change. Then, the surface stress state interchanges from tension to compression, and the center stress state interchanges from compression to tension. Until reaching T_{Keep1}, both surface and center stresses increase continuously. During keeping T_{Keep1}, the stresses at the surface and the center decrease because of the decreasing of temperature gradient. At the temperature of $T_{Bainite}$, bainite transformation occurs at the surface, causing a volume expansion and the surface compressive stress increases. To balance the increase of surface stress, the center tensile stress also increases. After the bainite phase transformation, the thermal contraction difference becomes larger and Young's modulus increases with decreasing temperature. Eventually, both surface and center residual stresses increase continuously.

Figure 5 shows the residual stress for HSS roll with $D = 600$ mm in Figure 1 in comparison with the previous experimental results σ_θ for HSS rolls with $D = 335$ mm,[16] D = 600–850 mm.[30] Here, it should be noted that the casting method and core material between roll in Figure 1 and HSS rolls with $D = 335$ mm, D = 600–850 mm are different. Although usually the different casting process and core material cause different residual stress, the residual stresses are nearly the same because of the following reasons. First, the effect of different casting method can be eliminated because of the pre-heating to the high temperature of T_{Start} before quenching. Second, the effect of different core materials is smaller during the same quenching process because thermal expansion properties are similar and only the pearlite transformation occurs for both materials during this process.[31] Third, the

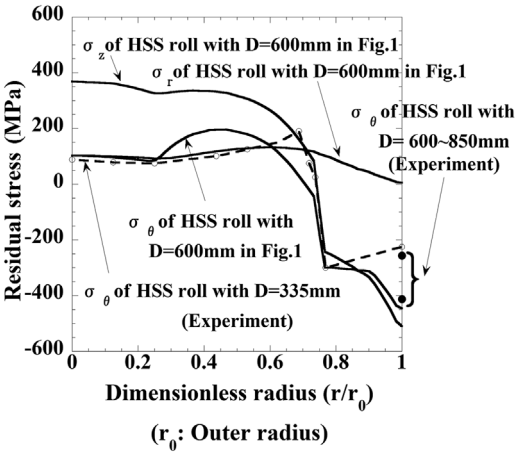

Figure 5. Simulation residual stress in comparison with the previous experimental results σ_θ of HSS roll with the steel shaft.[16,30]

effect of diameter on the residual stress was previously investigated by the roll industry and it was found that the surface residual stresses are similar when the rolls have the same diameter. The results in Section 4.1 in this paper also show that the surface residual stresses under the same roll diameter are almost independent of the shell–core ratio. Therefore, these three results can be compared, especially at the roll surface.

Figure 5 shows that simulation results at the center are close to the measuring results of the real roll. The simulation result is slightly larger than the experimental results, but they are almost coincided with each other except for the stress near the surface. This is probably because the stress relaxation due to tempering is not considered in this paper. In practically, it is known that the residual stress σ_z is the most important stress causing roll fracture or spalling during subsequent using process. Figure 5 also show that tensile stress σ_z at the center and compressive stress σ_z at the surface are larger than the other stresses σ_θ and σ_r, especially at the roll center. Therefore, the residual stress σ_z at the central cross section is mainly discussed in this paper.

4. Results and Discussion

4.1. Effect of shell–Core Ratio on Residual Stress

Because of the difference between the shell material and core material of the bimetallic roll, the component ratio of the shell and core influences roll performance. Hence, we should pay attention to the effect of shell–core ratio on residual stress. The equation of shell–core ratio is given as Equation 1:

$$\frac{A_s}{A_c} = \frac{D^2 - d^2}{d^2} \tag{1}$$

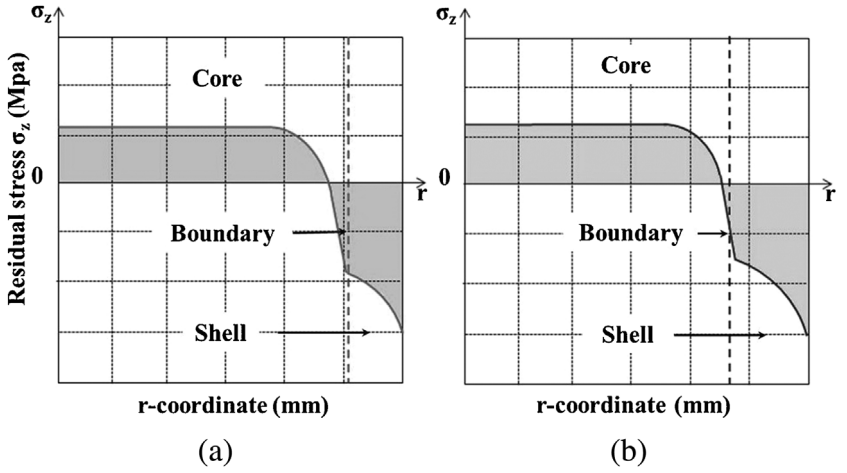

Figure 6. Schematic diagram of residual stress distribution: a) A_s/A_c = small and b) A_s/A_c = large.

where A_s is the shell area, A_c is the core area, D is the shell diameter, d is the core diameter.

During the hot strip rolling process, since the work roll is subject to severe thermal stress, it is necessary to grind the roll surface every time after a certain amount of wear appears. In addition, the oxidation, fire cracks, and sticking might sometimes occurring on the roll surface must be removed by grinding if troubles happen.[32] After being repeatedly polished, the shell thickness is gradually thinned until to the limit, then the roll becomes useless.

Although the larger shell–core ratio enhances roll service life under the same roll diameter, the larger tensile stress at center will be produced and causes risk of fracture. **Figure 6** shows a schematic illustration of the residual stress. It shows that under larger shell–core ratio, the larger tensile stress should appear at the core in order to balance the larger compressive region. Therefore, it has been thought that the larger shell–core ratio results in larger risk of fracture. To confirm the validity of this conventional conception, the effect of shell–core ratio on the residual stress will be discussed.

Figure 7 shows the residual stress distribution for different shell–core ratios when roll diameter $D = 600$ mm. Here, the analysis method and roll surface temperature are the same as the one in Figure 3. Although the A_s/A_c of the real roll lies in the range of 0.4–0.6, a larger range of 0.2–0.8 is chosen to clarify the effect. In Figure 6, the tensile residual stress at the center increases with increasing A_s/A_c. The tensile stress increases by 9% in the range of 0.2– 0.8, while only increases by 2% in the range of 0.4–0.6. The compressive stresses at the surface are almost unchanged. The results show that the shell–core ratio has a little influence on the residual stress of the bimetallic roll.

As shown in Figure 6, the compressive residual stress rapidly decreases from the surface to the boundary, and the compressive stress region does not increase with increasing A_s/A_c. As a result, the increasing of compressive stress region is smaller than the increase imaged conventionally. Therefore, the effect of shell–core ratio on the residual stress is less than expected result.

4.2. Effect of Roll Diameter on Residual Stress

Figure 8 shows the residual stress distribution of bimetallic roll with diameter $D = 500$–1000 mm at $A_s/A_c = 0.4$. Here, the analysis method and roll surface temperature are the same as the one in Figure 3. The center stress increases by 51% and the surface stress increases by 55% with increasing roll diameter. By contrast, the center stress increases by 13% and the surface stress increases 19% in the range of 600–800 mm of real roll. The results show that the roll diameter has a significant effect on the residual stress. However, the center stress decreases when $D = 900$–1000 mm. However, it can be found that the most of the maximum residual stress in the core occur at $r = d/2$.

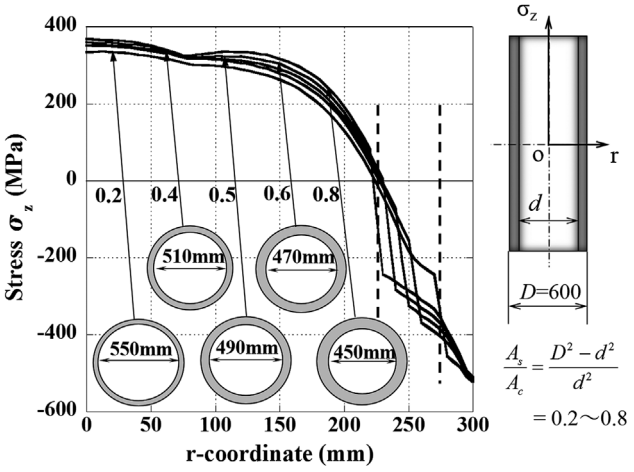

Figure 7. Distribution of residual stress σ_z for different A_s/A_c when $D = 600$ mm

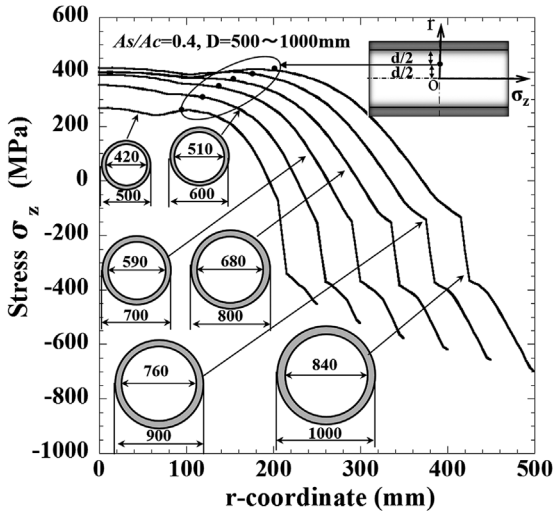

Figure 8. Distributions of residual stress σ_z of bimetallic roll for different D when $A_s/A_c = 0.4$.

The maximum residual stress is important for the evaluation of the roll strength. Therefore, we focus on this stress instead of the stress in the center. The stress at $r = d/2$ is shown in the solid circle ● in the Figure 8. It is seen that representative stress at $r = d/2$ increases with increasing roll diameter.

4.3. Effect of Phase Transformation on Residual Stress

During quenching process, the pearlite transformation occurs in the core material and bainite transformation occurs in the shell material. Volume expansions of core and shell happen with the phase transformations. The amount of expansion in the phase transformation has a significant effect on the residual stress. Therefore, the effect of the expansion on the residual stress will be discussed.

The solid lines in **Figure 9**(a) show the dilatometric curves of shell and core material during quenching

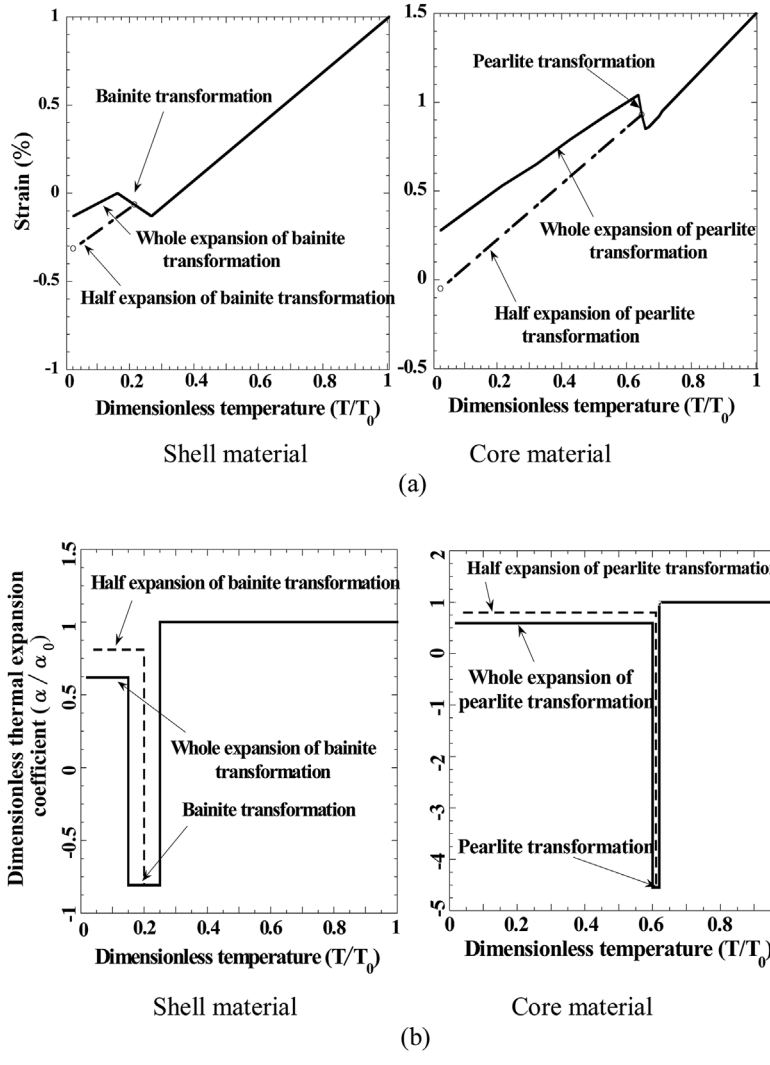

Figure 9. Thermal expansion of shell and core material during quenching: a) dilatometric curves and b) thermal expansion coefficients.

process, which is obtained from dilatometer experiment. In order to analyze the effect of the expansion on the residual stress quantitatively, the dilatometric curve with half amount of expansion is assumed. As shown by dotted lines in Figure 9(a), the starting point of the half expansion curve is assumed along the middle point of the beginning and ending point of the real phase transformation. The gradient of the half expansion curve is assumed as the middle value of the curves gradient before and after phase transformation. It should be noted that the changes of the others material properties caused by this half dilatometric curves are assumed to be ignored. In the simulation, the effect of expansion is expressed by thermal expansion coefficient.

Figure 9(b) shows the thermal expansion coefficients used as the input data of FEM, which is calculated based on dilatometric curves. The thermal expansion coefficient with the half expansion of pearlite transformation is called half pearlite (Half P) as well as the half bainite (Half B). The real thermal expansion coefficients are called real pearlite (Real P) and real bainite (Real B). In FEM analysis, only the thermal expansion coefficient will be changed and the other parameters remain unchanged.

The simulation is initially performed when the thermal expansion coefficients of shell and core material are changed together. **Figure 10**(a) shows the comparison of residual stress between Half P + Half B and Real P + Real B. The center stress increases by 24% and the surface stress increases by 60%. The result shows that phase transformation has a significant effect on the residual stress.

In order to clarify the distinct effect of pearlite transformation and bainite transformation, the half P and half B is performed independently. As show in Figure 10(b), the two cases are performed: (i) Half P + Real B; (ii) Real P + Half B.

In the case of Half P + Real B, the center stress increases by 76% and the surface stress increases by 41%. As shown in Figure 10(c), in the case of Half P, the center stress decreases by only half compared with the result of Real P. In addition, the tensile state of the surface is released because the expansion value of core material decreases. Therefore, the surface stress obviously decreases compared with the result of Real P at the ending of the pearlite transformation. As a result, the center tensile stress and the surface compressive stress obviously increases in the case of Half P + Real B. The results show that the pearlite transformation contributes to decreasing the residual stress.

In the case of Real P + Half B, the center stress decreases by 40% and the surface stress decreases by 33%. As shown in Figure 10(b), the stresses of center and surface are the same as the results of Real P + Real B before the bainite transformation. Since the surface stress is in tensile state when bainite transformation happens, the expansion will intensify this state and the surface stress will increase. Therefore, the tensile stress will decrease with decreasing expansion. In the case of Real P + Half B, the surface stress only increases by half compared with the result of Real P + Real B. As a result, the center tensile stress and the surface compressive stress obviously decreases in the case of Real P + Half B. The results show that bainite transformation results in increasing of residual stress.

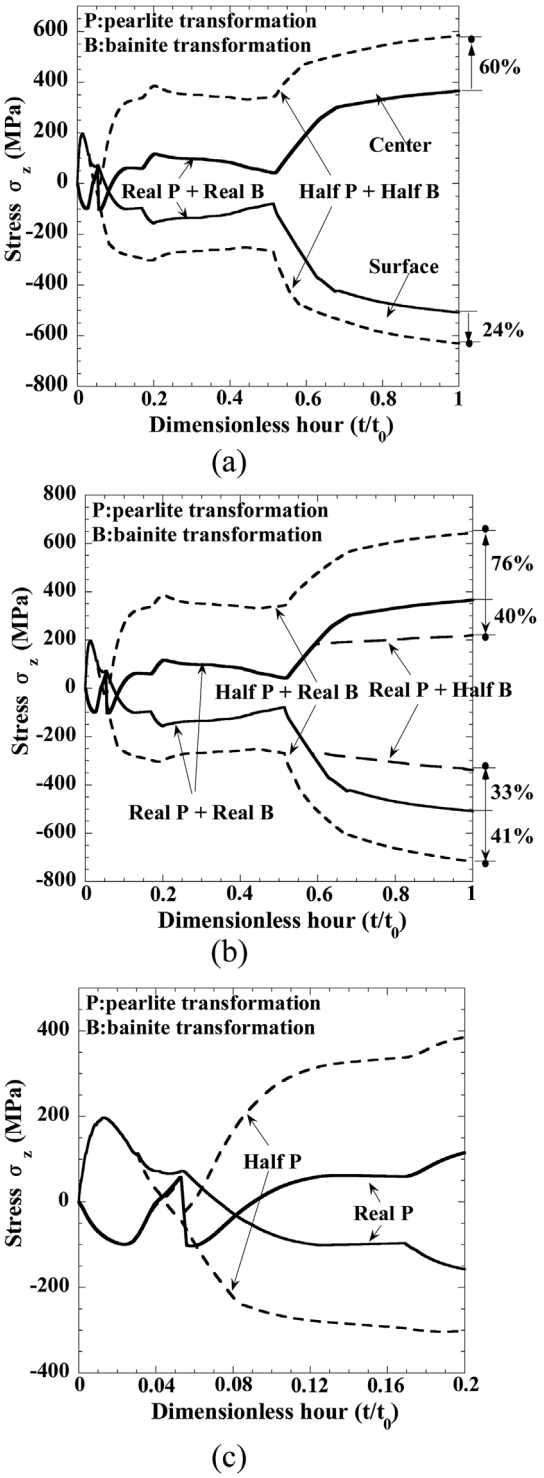

Figure 10. Effect of pearlite transformation and bainite transformation on residual stress: a) effect of Half P + Half B; b) effect of Half P + Real B and Real P + Half B; c) initial quenching.

4.4. Effect of Material's Heat Treatment on Residual Stress

Material property depends on heat treatment as well as the temperature. To ensure the simulation accuracy, the material properties should be distinguished in the heating process from room temperature and in the cooling process from T_{Start}. The tensile test of the cooling process from T_{Start} has been described in Section 3.2.1, and the heating process from room temperature is described as follows. The specimens were heated up to temperature testing temperature from room temperature with the speed of 500 °C h^{-1} and kept at this temperature for 20 min. The testing temperature of heating process includes room temperature, and 100 – T_{Start} at the interval of 100 °C.

In **Figure 11**, the stress-strain curves of the shell material at 600 °C are compared after heating from room temperature and cooling from T_{Start}. Here, σ_0 is the maximum stress corresponding to $\varepsilon = 0.65\%$ of the shell material at 600 °C after heating process from room temperature. In Figure 11 the maximum stress difference reaches 67% between the two heat treatment processes. It is found that the heat treatment significantly affects material mechanical property. The specimens were prepared from the shell of the roll that was quenched and tempered. The stress–strain curve indicated as "After heating process" in Figure 11 was obtained from the tensile test specimens after heated up to 600 °C from room temperature. In this case, although the specimens are tempered, the strength is not very much smaller than the strength under room temperature. On the other hand, the stress–strain curve indicated as "After cooling process" in Figure 11 was obtained from the tensile test specimens after heated up and cooled down from T_{Start} (about 1000 °C) to 600 °C by using the same cooling speed

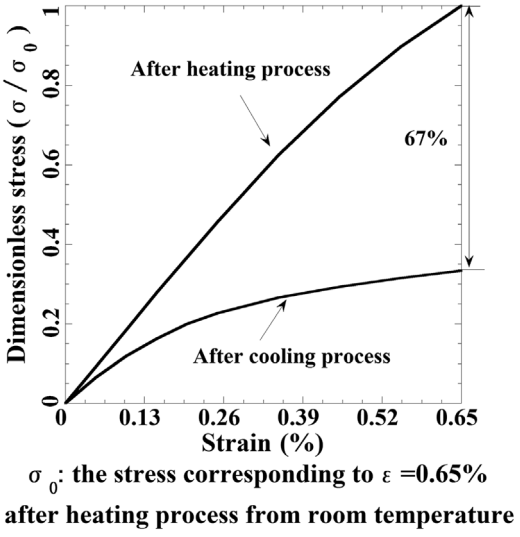

Figure 11. Stress–strain curves for the shell material at 600 °C after heating process from room temperature and cooling process from T_{Start}.

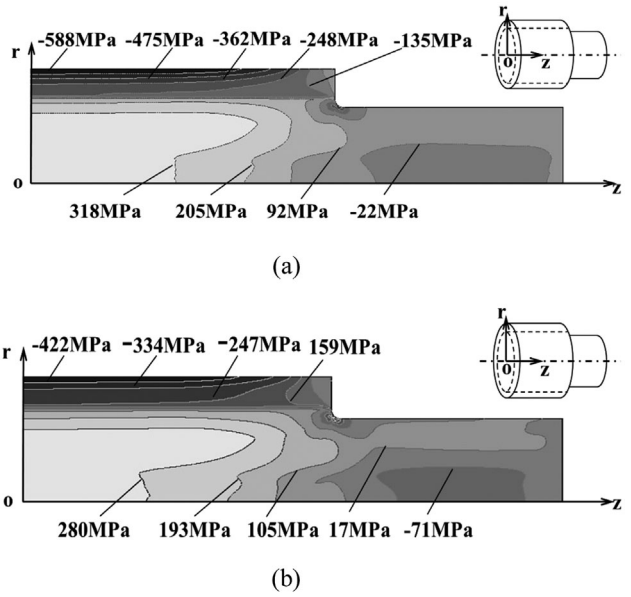

Figure 12. Contours of σ_z after quenching: a) using the heating process data and b) using the cooling process data.

of roll quenching. In this case, since the specimens are quenched, the material strength is similar to the strength of austenite state and therefore much smaller than the strength of "After heating process" in Figure 11.

Figure 12 shows the contours of residual stress σ_z after quenching. At the central cross section, the maximum compressive stress appears at the surface and the maximum tensile stress occurs at the center independent of the roll neck. Significant difference can be seen due to the data difference between cooling process form T_{Start} and heating process from room temperature.

Figure 13 shows the distribution of σ_z at $z = 0$. By using the cooling process data, the center stress decreases by 15% and the surface stress decreases by 27%. The residual stresses obtained from the cooling process data are similar

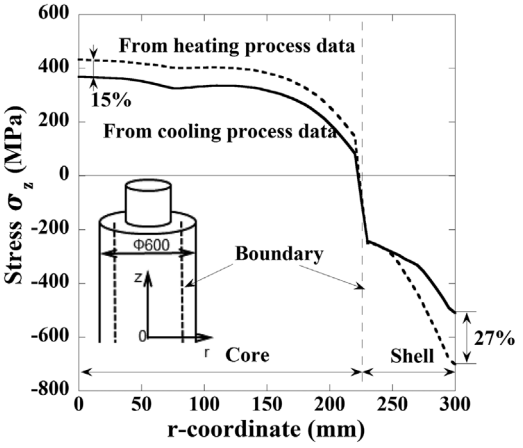

Figure 13. Distributions of residual stress σ_z obtained from heating process from room temperature and cooling process from T_{Start}.

to the results of HSS roll with the alloyed steel shaft.[33] Therefore, the necessity of cooling process data to the simulation is verified. However, the tensile stress of 368 MPa at the center and the compressive stress of 510 MPa at the surface are still larger than the previous result. In Figure 13, σ_z at the roll center reaches 430 MPa, which is larger than the yield stress 415 MPa given in Table 2. However, Mises equivalent stress at the same point is only 289 MPa, which is smaller than the yield stress.

5. Conclusions

In this paper, FEM analysis is performed to predict the residual stress generated during quenching for bimetallic work rolls using for hot strip rolling. The generation mechanisms of the residual stress have been discussed for single material roll and bimetallic roll. The results of the current study can be summarized as follows.

1. Predicting the residual stress of the bimetallic roll during quenching is realized by FEM simulation efficiently with lower cost and higher accuracy compared with experimental measurement. After quenching, the compressive stress appears at the shell while the tensile stress appears at the core.
2. The effect of shell–core ratio on the residual stress is very small. The center stress increases only by 2% and the surface stress is almost unchanged with increasing A_s/A_c from 0.4 to 0.6.
3. The roll diameter has a significant effect on the residual stress. The center stress increases by 13% and the surface stress increases by 19% with increasing the diameter from $D = 600$ to 800 mm. However, the center stress decreases with increasing from $D = 900$ to 1000 mm.
4. Phase transformation has a significant effect on the residual stress. Pearlite transformation contributes to decreasing the stress, while bainite transformation leads to increasing of stress.
5. Material properties depend on the heat treatment as well as the temperature. Therefore, by using the cooling process data, the center residual stress decreases by 15% and the surface residual stress decreases by 27% compared with the results by using the heating process data.

Acknowledgements

The authors gratefully acknowledge Hitachi Metals Ltd. for providing the material property of bimetallic rolls and the helpful discussions with this research. The authors also wish to express their thanks to the member of their group, Mr. X. Wang, Mr. W. H. Guan and Mr. Y. Nakagawa for their kind help in FEM simulation.

Received: November 22, 2015; Revised: February 3, 2016; Published online: March 21, 2016

Keywords: residual stress; work roll; quenching; FEM; hot rolling

References

[1] J. W. Choi, D. Kim, *ISIJ Int.* **1999**, *39* 823.
[2] H. Noguchi, Y. Watanabe, *Kawasaki Steel Giho*. **1987**, *19*, 195.
[3] M. Nilsson, M. Olsson, *Wear* **2013**, *307*, 209.
[4] K. Ichino, Y. Kataoka, T. Koseki, *Kawasaki Steel Tech. Rep.* **1997**, *37*, 13.
[5] M. Shimizu, O. Shitamura, S. Matsuo, T. Kamata, Y. Kondo, *ISIJ Int.* **1992**, *32*, 1244.
[6] H. G. Fu, A. M. Zhao, J. D. Xing, *J. Univ. Sci. Technol. Beijing* **2003**, *10*, 62.
[7] H. Takigawa, T. Tanaka, S. Ohtomo, *Nippon Steel Tech. Rep.* **1997**, *74*, 77.
[8] H. G. Fu, H. J. Zhao, Z. Z. Du, Z. J. Feng, Y. P. Lei, Y. Zhang, M. W. Li, Y. H. Jiang, R. Zhou, H. X. Guo, *Ironmaking Steelmaking* **2011**, *38*, 338.
[9] Jr. M. Boccalini, A. Sinatora, *Proc. of 6th Int. Tooling Conference*. Karlstads University, Karlstad, **2002**, 425.
[10] L. D. V. Z. VRO, E. Valjanje, *Mater. Tehnol.* **2014**, *48*, 983.
[11] B. Podgornik, S. Milanović, J. Vižintin, *J. Mater. Proc. Technol.* **2010**, *210*, 1083.
[12] C. F. Onisa, D. C. J. Farrugia, *Int. J. Mate. Form.* **2008**, *1*, 363.
[13] A. Pérez, R. L. Corral, R. Fuentes, R. Colás, *J. Mater. Process. Technol.* **2004**, *153*, 894.
[14] D. Benasciutti, *J. Strain Anal.* **2012**, *47*, 297.
[15] D. F. Chang, *J. Mater. Proc. Technol.* **1999**, *94*, 45.
[16] Y. Sano, T. Hattori, M. Haga, *ISIJ Int.* **1992**, *32*, 1194.
[17] G. S. Schajer, *Practical Residual Stress Measurement Methods*, John Wiley & Sons, Hoboken, **2013**, *7*.
[18] E. Kingston, D. J. Smith, *Ironmaking Steelmaking* **2005**, *32*, 379.
[19] G. Sachs, *Zeit Metallkunde.* **1927**, *19*, 352.
[20] Y. Higashida, T. Kikuma, *Tetsu-to-Hagane.* **1986**, *72*, 308.
[21] C. Neto, *34th Mechanical Working and Steel Processing Conference Proceedings*. Iron and Steel Society, Warrendale, **1993**, 199.
[22] J. Pacyna, A. Kokosza, A. S. Wojtas, *J Nondestr Test Ultrason.* **1999**, *4*, 8.
[23] J. Yasuhiro, *33th Mechanical Working and Steel Processing Conference*. Iron and Steel Society, Warrendale, **1992**, 187.
[24] S. H. Kang, Y. T. Im, *J. Mater. Proc. Technol.* **2007**, *192*, 381.

[25] S. Kamamoto, T. Nishimori, S. Kinoshita, *Mater. Sci. Technol.* **1985**, *1*, 798.
[26] A. Majorek, B. Scholtes, H. Muller, E. Machrauch, *Steel Res.* **1994**, *65*, 146.
[27] H. M. Cheng, X. Q. Huang, H. G. Wang, *J. Mater. Process. Technol.* **1999**, *89*, 339.
[28] I. Neira Torres, G. Gilles, J. Tchoufang Tchuindjang, J. Lecomte-Beckers, M. Sinnaeve, A. M. Habraken, *Adv. Mater. Res.* **2014**, *996*, 580.
[29] ASTM E831-14, *Standard Test Method for Linear Thermal Expansion of Solid Materials by Thermomechanical Analysis*, ASTM International, West Conshohocken, PA, **2014**.
[30] O. Shitamura, H. Kodama, Y. Sano, *Hitachi Rev.* **1990**, *39*, 231.
[31] Z. J. Chen, J. Zhang, L. Yu, G. J. Huang, *Mater. Res.* **2014**, *17*, 1601.
[32] Y. Sekimoto, Y. Sugimura, K. Hirata, *Hitachi Giho.* **1968**, *50*, 549.
[33] A. Noda, E. Matsunaga, T. Hattori, Y. Sano, *Hitachi Giho.* **1997**, *13*, 89.